PAPER

Investigations on Nb$_2$C monolayer as promising anode material for Li or non-Li ion batteries from first-principles calculations

Junping Hu,[abce] Bo Xu,[d] Chuying Ouyang,[d] Ying Zhang*[f] and Shengyuan A. Yang*[c]

First-principles calculations are performed to study the electronic properties and metal ion storage capabilities of the two-dimensional (2D) Nb$_2$C monolayer and its corresponding fluoride and hydroxide materials. We show that the Nb$_2$C monolayer and the derived Nb$_2$CF$_2$ and Nb$_2$C(OH)$_2$ are all metallic in their most stable configurations. We systematically investigate the adsorption and surface diffusion of different metal atom species A = Li, Na, K, Be, Mg, Ca, Al. We find that the bare Nb$_2$C monolayer has excellent performance in the case of Li or Mg: the material remains metallic after adsorption; the ion diffusion is fast with extremely low diffusion barrier; the storage capacity is high ($\sim$542 mA h g^{-1} for Li and $\sim$1084 mA h g^{-1} for Mg); and the average intercalation potential is relatively low. Particularly, the diffusion barrier heights for the elements Li, Na, K, Mg and Ca are all lower than 0.1 eV. In addition, the functional groups tend to strongly degrade the performance, which should be avoided in experiment as much as possible. Our results suggest that the Nb$_2$C monolayer is a promising anode material for Li- or non-Li-ion batteries.

1   Introduction

From portable electronic devices to electric vehicles and to large-scale power grid systems, energy storage has become an essential technology for our daily life. Among all kinds of energy storage systems, secondary batteries have the important advantages of high efficiency and compactness.[1–3] As the most prominent example, Li-ion batteries (LIBs) have undergone rapid development since their first commercialization by Sony in 1991. Nevertheless, currently the development of LIBs has been hampered by cost and safety issues.[4] With the increasing usage of LIBs, the lack of lithium sources also emerges as one major challenge. Therefore, non-Li-ion batteries, in which Li is substituted by other metal species, are being actively explored. Particularly, Na-ion batteries (NIBs) have received a lot of attention because Na is much more abundant and cheaper than lithium.[5,6] Beyond NIBs, batteries with other alkali (such as K)[7,8] or multivalent metal ions (Mg,[9,10] Ca,[11] and Al[12]) have also been investigated. For developing all these various secondary

batteries, a critical problem is to search for suitable electrode materials to optimize the battery performance.

Since the discovery of graphene, the novel properties and wide applications of two-dimensional (2D) layered materials have attracted tremendous interest. 2D materials such as graphene, phosphorene and dichalcogenides (such as NbSe$_2$ and MoS$_2$)[13–15] have been investigated as electrode materials for LIBs,[16–22] and the MoS$_2$/graphene 2D composite has also been tested as anode materials for NIBs.[23] Recently, a new family of 2D materials, the early transition-metal carbides and carbonitrides (M$_{n+1}$X$_n$, n = 1, 2, 3; X = C or N), known as "MXenes", have attracted more and more attention in research. MXenes are typically synthesized from the MAX precursors (A represents one of the A group elements such as Al), which include more than 60 phases. One of the MXenes, Ti$_3$C$_2$, was first synthesized by Naguib *et al.*[24–27] by selectively etching the Al layers from Ti$_3$AlC$_2$ with hydrofluoric acid (HF). To date, many other MXenes have also been successfully synthesized, such as Ti$_3$CN, Ti$_2$C, (V$_{0.5}$Cr$_{0.5}$)$_3$C$_2$, (Ti$_{0.5}$Nb$_{0.5}$)$_2$C, Nb$_2$C, V$_2$C and Ta$_4$C$_3$, *etc.*[25–29]

With more MXenes being realized, their properties have been actively studied.[30–34] It has been shown that these materials could have great potential for energy storage applications. For instance, Zhou *et al.*[35] proposed that monolayer Ti$_3$C$_2$ and its derivatives are promising anode materials for LIBs using first-principles calculations. Naguib *et al.* theoretically predicted that Ti$_2$C, (Ti$_{0.5}$Nb$_{0.5}$)$_2$C, Ti$_3$(C$_{0.5}$N$_{0.5}$), Ti$_3$CN, TiNbC, Nb$_2$C and Ta$_4$C$_3$ are all suitable electrode materials for LIBs.[36,37] Gogotsi *et al.* demonstrated that 2D Ti$_3$C$_2$ MXene layers could be spontaneously intercalated by Na$^+$, K$^+$, NH$_4^+$, Mg^{2+} and Al^{3+} ions.[38] They also

a School of Physics, Beijing Institute of Technology, Beijing 100081, China

b School of Science, Nanchang Institute of Technology, Nanchang 330099, China

c Research Laboratory for Quantum Materials, Singapore University of Technology and Design, Singapore 487372, Singapore. E-mail: shengyuan_yang@sutd.edu.sg

d Department of Physics, Jiangxi Normal University, Nanchang 330022, China

e Kunming Institute of Physics, Kunming, Yunnan 650223, China

f Department of Physics, Beijing Normal University, Beijing 100875, China. E-mail: yingzhang@bnu.edu.cn

performed calculations and showed that the MXene nanosheet could be utilized as anodes for non-Li-ion batteries.[39]

In recent experiments, two new kinds of MXenes (V_2C, Nb_2C) have been successfully synthesized for the first time by treating their corresponding MAX phases (V_2AlC, Nb_2AlC) in aqueous HF.[40] Preliminary experimental studies demonstrated that for V_2C-based electrodes, reversible capacities of 260 mA h g^{-1} at 1C and 125 mA h g^{-1} at 10C could be achieved; while for Nb_2C-based electrodes, 170 mA h g^{-1} at 1C and 110 mA h g^{-1} at 10C were obtained. The measured Li specific capacities are not high enough as expected. For V_2C, later on, it was clarified that the high capacity of bare V_2C might be decreased largely by the functional groups which remain after synthesis.[41] Whether a similar scenario also occurs in the case of Nb_2C is currently not fully understood. In addition, it is worth noting that from low to high charge–discharge rates the capacity of Nb_2C-based electrodes decreases much slower than the V_2C-based electrodes, implying a much faster ion diffusion for Nb_2C. Furthermore, since Nb belongs to the 4d transition metals, the electronic correlation effects could strongly affect the material's chemical and physical properties. All these interesting observations call for a detailed theoretical study to fully investigate the properties of Nb_2C-based 2D materials.

Motivated by the reasons stated above, in this paper, we systematically investigate the electronic and metal ion storage properties of the Nb_2C monolayer and its fluorinated and hydroxylated derivatives as anode materials based on first-principles calculations. We determine the structural and electronic properties of the materials before and after adsorption. The adsorption and diffusion of different metal species A (A = Li, Na, K, Be, Mg, Ca, Al) are studied. We find that the bare Nb_2C monolayer has very good performance as an anode material. Especially, its surface diffusion barrier heights for various ions are all below 0.1 eV which is among the lowest of all the existing 2D materials discovered to date, indicating a very fast ion diffusion. We also show that the bare Nb_2C monolayer is metallic before and after adsorption, with a very high specific Mg capacity ($\sim$1084 mA h g^{-1}) as well as a high Li capacity ($\sim$542 mA h g^{-1}). The functional groups greatly reduce the Li or non-Li storage capacities, which should be avoided in experiment as much as possible.

2   Computational details

Our calculations are based on density functional theory (DFT) using the plane-wave pseudopotentials[42] with the Perdew–Burke–Ernzerhof (PBE)[43,44] form of exchange–correlation functionals as implemented in the Vienna Ab initio Simulation Package (VASP).[45] A cutoff energy of 600 eV is employed for the plane wave expansion. Considering the strong correlation effects in niobium element, electronic structure calculations and structural relaxations are performed by using a GGA plus Hubbard U (GGA+U)[46,47] method. The U value of the Nb atom is set to be 6.5 eV.[48] The Brillouin zone is sampled with 6 × 6 × 1 Monkhorst–Pack k-point mesh[49] for the structural optimization, and with 12 × 12 × 1 mesh for the electronic structure calculations. The

convergence criteria for the total energy and ionic forces were set to be 10^{-4} eV and 0.001 eV Å^{-1}, respectively.

Possible spin polarization is carefully tested and no spin-polarization effect is observed in our calculation. In addition, concerning the spin–orbital coupling (SOC) effects, we have compared the electronic structures of Nb_2C monolayer with and without SOC in our calculations. Results show that the SOC effect has little effect on the band structure. Therefore, in the following calculations we do not include the SOC effect.

The atomic model of the free-standing Nb_2C sheet constructed based on the Nb_2AlC structure is used as the initial configuration for geometry optimization. Each bare Nb_2C monolayer consists of a triple-layer stacked in the sequence of Nb(1)–C–Nb(2), which can be viewed as two Nb-atomic layers being cleaved with one C-atomic layer, forming edge-shared Nb_2C octahedra [Fig. 1(a)]. For the study of metal ion adsorption and diffusion on Nb_2C and Nb_2CX_2 (X = F, OH) monolayers, a 4 × 4 supercell containing 32 Nb and 16 C atoms is employed in

Fig. 1 Optimized lattice structure of bare Nb_2C monolayer and its fluorinated and hydroxylated derivatives. (a) Side view and (b) top view of the bare Nb_2C monolayer consisting of a triple atomic layer with Nb(1)–C–Nb(2) stacking sequence. (c–h) Side views of the lattice structures of (c) I-Nb_2CF_2, (d) II-Nb_2CF_2, (e) III-Nb_2CF_2, (f) I-$Nb_2C(OH)_2$, (g) II-$Nb_2C(OH)_2$ and (h) III-$Nb_2C(OH)_2$. (i and j) Top views of I-Nb_2CF_2 and II-Nb_2CF_2, in which the F groups are on top of the C atoms or above the hollow sites formed by three neighboring C atoms, respectively. III-Nb_2CF_2 is a combination of I-Nb_2CF_2 and II-Nb_2CF_2, in which the F groups are located above the C atoms on one side and at the hollow sites on the other side. The geometric configurations of OH groups for I-$Nb_2C(OH)_2$, II-$Nb_2C(OH)_2$ and III-$Nb_2C(OH)_2$ resemble those of the corresponding fluorides shown in the figure.

our calculations. A 2×2 supercell is utilized for the study of structural and electronic properties, average open circuit voltage, and storage capacity.

3   Results and discussion

3.1   Structural and electronic properties of Nb$_2$C and Nb$_2$CX$_2$ (X = F, OH) monolayers

We first address the optimized crystal structures and the electronic properties of monolayer Nb$_2$C as well as its fluorinated and hydroxylated derivatives [denoted as Nb$_2$CF$_2$ and Nb$_2$C(OH)$_2$, respectively]. For a 2×2 supercell of the bare Nb$_2$C monolayer, the optimized lattice parameters are listed in Table 1. The vertical distance between Nb(1)-layer and Nb(2)-layer, *i.e.*, the thickness of the monolayer, is 2.468 Å. The Nb(1)–C bond length is 2.198 Å, the same as that of the Nb(2)–C bond.

The Nb$_2$CF$_2$ and Nb$_2$C(OH)$_2$ sheets are constructed by saturating the surface under-coordinated Nb atoms with F and OH, respectively. Three possible configurations are considered: type I: the F or OH groups are above the vertical site of each C atom on both sides of the Nb$_2$C monolayer [see Fig. 1(c) and (f)]; type II: the F or OH groups are located above each hollow site formed by three neighboring C atoms on both sides of the Nb$_2$C monolayer [see Fig. 1(d) and (g)]; type III: a mixture of type I and II, in which the F or OH groups are located above the vertical sites of three C atoms on one side while above the hollow sites of C atoms on the other side, forming different layouts on the two sides of the Nb$_2$C monolayer [see Fig. 1(e) and (h)]. The optimized lattice parameters for each type of configuration are shown in Table 1.

The relative structural stability of the three types of configurations for Nb$_2$CF$_2$ and Nb$_2$C(OH)$_2$ can be determined by comparing their total energies. The results show that the type I configuration is energetically the most favorable for both Nb$_2$CF$_2$ and Nb$_2$C(OH)$_2$. Specifically, the total energy of I-Nb$_2$CF$_2$ (denoting the type I structure) is lower than that of II-Nb$_2$CF$_2$ and III-Nb$_2$CF$_2$ by about 0.17 and 0.55 eV per unit cell, respectively. Also, the energy of I-Nb$_2$C(OH)$_2$ is lower than that of II-Nb$_2$C(OH)$_2$ and III-Nb$_2$C(OH)$_2$ by about 0.24 and 0.51 eV per unit cell, respectively. This indicates that both F and OH groups prefer to stay at the top sites of C atoms, rather than staying at the hollow sites. It is also worth noting that for both

derivatives, their type I structures have the largest lattice parameter and the thinnest layer thickness.

In order to be utilized as battery electrode materials, it is desirable for the material to be metallic. Fig. 2 shows the total density of states (DOS) of Nb$_2$C, Nb$_2$CF$_2$ and Nb$_2$C(OH)$_2$ monolayers. For bare Nb$_2$C, the resulting DOS in Fig. 2(a) indicates that it is metallic, which is in agreement with previous work.[50] We find that when Nb$_2$C is passivated by F or OH, the generated Nb$_2$CF$_2$ or Nb$_2$C(OH)$_2$ monolayers still maintain metallic properties regardless of the specific adsorption configurations [see Fig. 2(b)–(g)]. This hence indicates that the
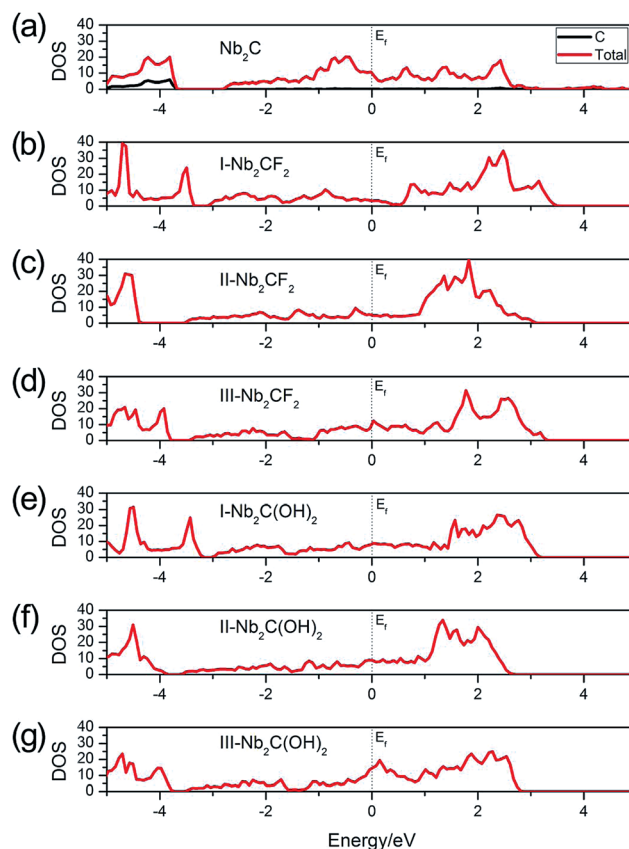

Fig. 2   Total DOS of (a) Nb$_2$C, (b) I-Nb$_2$CF$_2$, (c) II-Nb$_2$CF$_2$, (d) III-Nb$_2$CF$_2$, (e) I-Nb$_2$C(OH)$_2$, (f) II-Nb$_2$C(OH)$_2$ and (g) III-Nb$_2$C(OH)$_2$. The Fermi levels are set to zero.

Table 1   The optimized structural parameters for the bare Nb$_2$C monolayer and its fluorinated and hydroxylated derivatives. The lengths are in Å

	Parameter	Bond length		Thickness
	a, b	Nb(1)–C/Nb(2)–C	Nb(1)–F/O/Nb(2)–F/O	Monolayer
Nb$_2$C	6.302	2.198/2.198		2.468
I-Nb$_2$CF$_2$	6.526	2.188/2.188	2.335/2.335	4.984
II-Nb$_2$CF$_2$	6.100	2.227/2.227	2.270/2.270	5.592
III-Nb$_2$CF$_2$	6.200	2.250/2.164	2.289/2.326	5.492
I-Nb$_2$C(OH)$_2$	6.500	2.197/2.197	2.231/2.231	6.979
II-Nb$_2$C(OH)$_2$	6.176	2.237/2.237	2.261/2.261	7.435
III-Nb$_2$C(OH)$_2$	6.280	2.255/2.174	2.275/2.322	7.326

bare Nb_2C monolayer and its fluorinated and hydroxylated derivatives all satisfy the requirement of being metallic for electrode materials. Fig. 2(a) also shows that the C atoms have almost no contribution to states near the Fermi level, namely, the low-energy carriers are originated from Nb atoms. We note that neglecting the correlation effect on Nb atoms would lead to insulating phases for the two derivatives,[40] which indicates the importance of electronic correlation effects in the current system. Due to the above analysis, we will mainly focus on the most stable structures, *i.e.* the type I structures for the two derivatives Nb_2CF_2 and $Nb_2C(OH)_2$ in the following investigations.

3.2 Metal atom adsorption on Nb_2C and on Nb_2CX_2 (X = F, OH) monolayers

Since the Nb_2C monolayer and its fluorinated or hydroxylated derivatives are all metallic, in the following, we explore the possibility of these materials to be utilized as electrode materials for Li- and non-Li-ion batteries by investigating their adsorption of the metal species A (A = Li, Na, K, Be, Mg, Ca, Al). To this end, the first step is to analyze the adsorption energy and to determine the most favorable adsorption site. Herein, a 4 × 4 supercell is used to study the adsorption of one A atom on the surface, corresponding to the chemical stoichiometries of $Nb_{32}C_{16}A$, $Nb_{32}C_{16}F_{32}A$ and $Nb_{32}C_{16}(OH)_{32}A$, respectively, for the three materials. Three different adsorption sites with high symmetry are considered in our calculations: (i) top site of C atom (which is above the F atom for I-Nb_2CF_2, and above the OH group for I-$Nb_2C(OH)_2$); (ii) top site of Nb(1) atom; (iii) top site of Nb(2) atom.

Here, the adsorption energy (E_{ad}) of an A atom on the monolayer is defined as:

$$E_{ad} = E_{Nb_{32}C_{16}X_{32}A(X=\square,F,OH)} - E_{Nb_{32}C_{16}X_{32}(X=\square,F,OH)} - E_A, \quad (1)$$

where E_A is the energy per atom in the bulk metal of A, $E_{Nb_{32}C_{16}X_{32}A(X=\square,F,OH)}$ and $E_{Nb_{32}C_{16}X_{32}(X=\square,F,OH)}$ are the total energies of the $Nb_{32}C_{16}X_{32}$ (X = $\square$, F, OH) monolayer with and without A adsorption. The symbol "$\square$" here means the bare monolayer without functional groups.

A negative value of E_{ad} indicates that the corresponding atom A prefers to adsorb on the monolayer, instead of forming a metal cluster. The adsorption energies calculated for different adsorption sites are plotted in Fig. 3. One observes that for I-Nb_2CF_2, only Na and K can adsorb on the monolayer (for Na, only the top site of Nb(2) works), while other adatoms tend to form metal clusters by themselves. For I-$Nb_2C(OH)_2$, all the adsorption energies are positive indicating that none of the atoms can get adsorbed. Therefore the presence of F/OH groups on the surface would significantly degrade the storage capacity of Nb_2C. This is similar to the cases of other MXene materials.[35,41]

Fortunately, for the bare Nb_2C monolayer, almost all the adatoms prefer to adsorb on its surface as indicated by the negative adsorption energy values in Fig. 3(a), except for Be and Al which have relatively small E_{ad}. The result indicates that the bare Nb_2C monolayer possesses the possibility to be utilized as an electrode material for the A'-ion batteries with (A' = Li, Na, K, Mg, Ca). Further, by comparing the adsorption energies for different sites, one can determine the most favorable adsorption site for each element. Specifically, the most favorable adsorption sites for Li, Na, K, Mg and Ca are on top of C, Nb(2), Nb(2), C and C, respectively. In the following calculations, we will focus on the adsorption of Li, Na, K, Mg and Ca atoms onto the bare Nb_2C monolayer.

We next present the optimized structures for A'-adsorbed Nb_2C monolayers (A' = Li, Na, K, Mg, Ca). As shown in Fig. 4, for the cases of Na- and K-adsorption, the distances along the c-axis between Nb(2) and Na/K (or between C and Na/K) are 5.209/

Fig. 3 Adsorption energies for atom species A (A = Li, Na, K, Be, Mg, Ca, Al) on (a) Nb_2C, (b) I-Nb_2CF_2 and (c) I-$Nb_2C(OH)_2$ at different adsorption sites.

Fig. 4 Side views of the optimized structures of Nb_2C monolayers after adsorption with (a) Li, (b) Na, (c) K, (d) Mg and (e) Ca.

Table 2 Bader charge analysis. The number of valence electrons taken into account in the calculation for Li, Na, K, Mg, Ca, Nb and C are 1, 1, 9, 2, 10, 13 and 4, respectively

	Average charge state		
	Nb	C	A$'$
Nb_2C	11.91	6.18	
Nb_2C + Li	12.02	6.18	0.16
Nb_2C + Na	11.99	6.18	0.32
Nb_2C + K	11.99	6.18	8.32
Nb_2C + Mg	12.00	6.17	1.31
Nb_2C + Ca	12.03	6.17	9.06

5.620 Å (or 3.978/4.391 Å), respectively. The adsorption height of K is larger than that of Na. For Li-, Mg- and Ca-adsorbed configurations, the distances along the c-axis between C and Li/Mg/Ca are 3.677/3.678/3.981 Å, respectively. To further investigate the charge transfer during the adsorption process, we carry out the Bader charge analysis. The results are listed in Table 2. One can see that in general the adatoms lose electrons, which are mostly transferred to the C atoms in the layer. To be specific, the Li atom transfers about 0.84e to the bare Nb_2C monolayer, and the transferred charges for Na/K/Mg/Ca are about 0.68/0.68/0.69/0.94e, respectively. This indicates that the atoms are chemically adsorbed on Nb_2C and they form chemical compounds, corresponding to the redox reaction similar to other electrode materials.

After adsorption, whether the monolayer would maintain a metallic character or become an insulator is important for its electrode performance. To answer this question, we calculate the total DOS of the A$'$-adsorbed Nb_2C monolayer. The results are shown in Fig. 5. We can see that, as desired for a good electrode material, the system remains metallic after adsorption with any kind of the A$'$ atoms (A$'$ = Li, Na, K, Mg, Ca).

3.3 Ion diffusion on Nb_2C monolayer

Next, we turn to study the ion diffusion of A$'$ (A$'$ = Li, Na, K, Mg, Ca) on the surface of the Nb_2C monolayer. The climbing-image
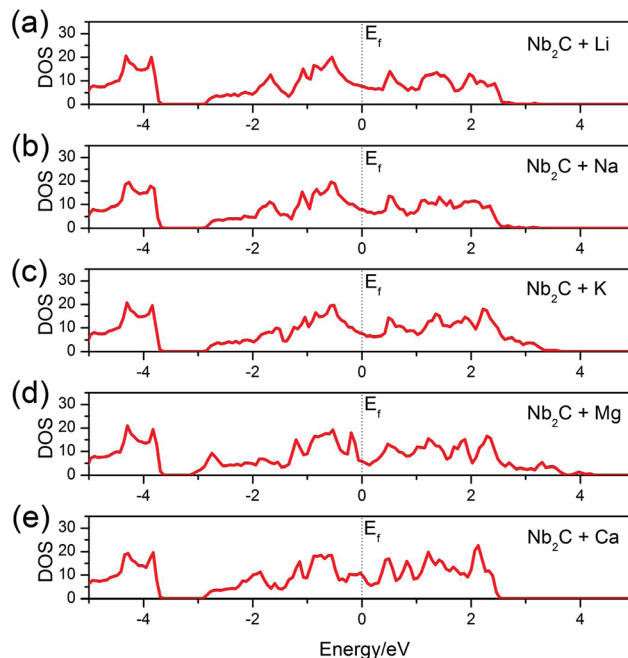

Fig. 5 Total DOS of the bare Nb_2C monolayer after (a) Li, (b) Na, (c) K, (d) Mg and (e) Ca adsorption. The dotted vertical lines denote the Fermi levels.

nudged elastic band (NEB) method[51] is used to seek the saddle points and the minimum energy path and to determine the diffusion barrier height. The most stable adsorption configuration (which is determined for each atom species in the previous section) is taken as the initial state. The configurations with A$'$ adsorption at the nearest-neighboring most stable site is chosen to be the final state. Fig. 6 shows the calculated diffusion energy profiles and the corresponding migration pathways. Our results show that the diffusion barriers are 0.032 eV (for Li), 0.015 eV (for Na), 0.004 eV (for K), 0.096 eV (for Mg) and 0.039 eV (for Ca), respectively. These low energy barriers indicate fast ion diffusion. For Li, Mg and Ca [Fig. 6(a), (e) and (f)], the diffusion paths are almost the same, from the T_1 site to the neighboring T_1' site passing through the T_2' site [see Fig. 6(c)]. These paths clearly show two saddle points. For Na and K, their diffusion paths are from T_2 to T_2'. The path for Na has two saddle points and it passes through the T_3 site. Meanwhile, one observes that the path for K goes from T_2 to T_2' almost directly with only one saddle point located, which might be due to its very small barrier height (0.004 eV). Overall, the diffusion barrier heights are very low, indicating that all the A$'$ atoms could have fast diffusion on the surface of the Nb_2C monolayer, which is advantageous for applications as electrode materials.

We stress that all these diffusion barrier heights are less than 0.1 eV, which are among the lowest of the available anode materials. For example, in terms of diffusion barrier heights, we have for Ti_3C_2 (0.068 eV for Li,[3,35] 0.096 eV for Na, 0.103 eV for K and 0.118 eV for Ca[3]), silicene (0.28 eV for Li,[52] 0.25 eV for Na,[53] 0.11 eV for K[54]), graphene[55,56] (>0.3 eV for Li, ~0.10 eV for Na, K, Mg, Ca, Al[57,58]), phosphorene (0.13–0.76 eV for Li,[59,60] 0.04 eV for Na,[61] 0.30 eV for Mg and 0.69 eV for Al[62]), Mo_2S (0.21 eV for Li,[21]
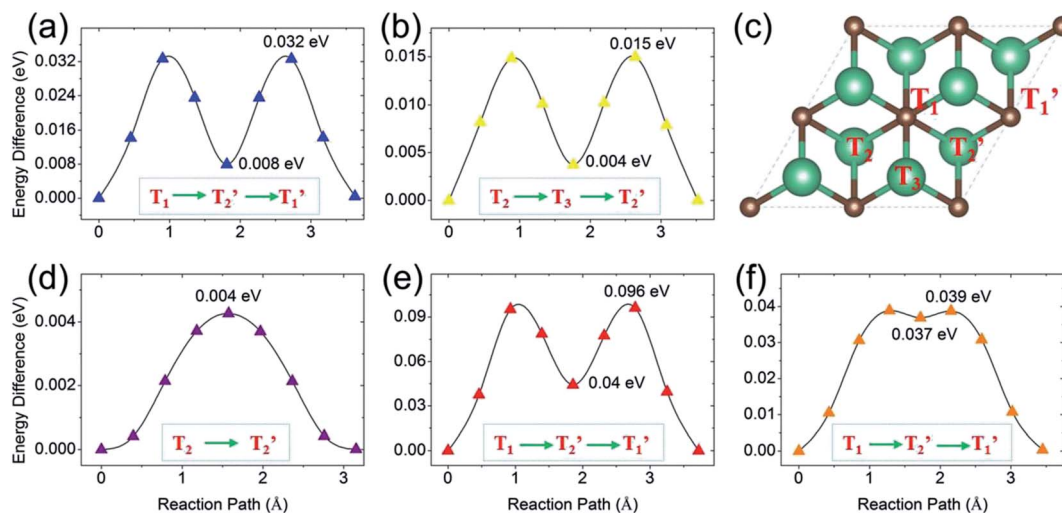
Fig. 6 The diffusion barrier profiles of (a) Li, (b) Na, (d) K, (e) Mg and (f) Ca on the Nb_2C monolayer. The migration paths for A′ diffusion are shown in the inset of each panel. (c) labelling of the high symmetry points appearing in the diffusion paths. T_1 and T_1' represent the two sites on top of two neighboring C atoms. T_2 and T_2' represent the two sites on top of two neighboring Nb(2) atoms. T_3 represents the site on top of the Nb(1) atom.

0.28 eV for Na,[63] 0.48 eV for Mg[64]), TiO_2-based polymorphs (0.3–0.65 eV for Li,[65,66] 0.4 eV for Na[67]), and the commercialized graphite (0.2–0.4 eV for Li[68]). All these are larger than the corresponding values of Nb_2C.

Experimentally it has been found that the reversible capacities of the Nb_2C-based electrode are 170 and 110 mA h g^{-1} obtained at 1C and 10C respectively, while for V_2C-based electrode, the two values are 260 and 125 mA h g^{-1} respectively.[40] The reversible capacity of Nb_2C-based electrodes is 65% of that of V_2C-based electrode at 1C, and this percentage is increased to 88% at 10C. According to our results above, the experimental observation might be attributed to the faster Li diffusion on Nb_2C surface than on V_2C surface (barrier height $\sim$ 0.045 eV for V_2C[41]).

3.4 Average open circuit voltage and storage capacity of Nb_2C monolayer

The average open circuit voltage and the storage capacity are important characteristics for battery electrode materials. To estimate the maximum possible capacity for A′ atom adsorption, we still employ the 2×2 supercell and increase concentration of A′ atoms adsorbed on both sides of the host Nb_2C monolayer. Here we assume the following half-cell reaction vs. A′/A′$^+$:[69,70]

$$Nb_2C + xA'^{y+} + xye^- \leftrightarrow Nb_2CA'_x. \quad (2)$$

The difference in total energies before and after A′ intercalation is used to determine the average open circuit voltage. The volume and entropy effects are usually negligible during the reaction. The average open circuit voltage can be approximately computed from the energy difference:

$$V_{ave} = (E_{Nb_2C} + xE_{A'} - E_{Nb_2CA'_x})/xye \quad (3)$$

where E_{Nb_2C} and $E_{Nb_2CA'_x}$ are the total energies of Nb_2C without and with A′ intercalation, and $E_{A'}$ is the energy per atom in the bulk metal A′.

We first take the Li case as an example to demonstrate the calculation of the average open circuit voltage and the storage capacity. In this case, the adsorption sites of the first Li layer are at the top sites of C atoms, because they correspond to the most stable sites for Li adsorption onto the bare Nb_2C monolayer. From symmetry, the Li layer could form on both sides of the Nb_2C monolayer. After the first-layer adsorption, the second layer Li atoms are adsorbed on the top sites of Nb(2) atoms (also on both sides). To evaluate the interaction between the host material and the Li layers, we calculate the layer-resolved average adsorption energy (E_{ave}^n) of Li atoms in the n-th layer, which is defined as

$$E_{ave}^n = (E_{Nb_8C_4Li_{n\times8}} - E_{Nb_8C_4Li_{(n-1)\times8}} - 8E_{Li})/8, \quad (4)$$

where E_{Li} is the energy per atom in the bulk metal Li, $E_{Nb_8C_4Li_{n\times8}}$ and $E_{Nb_8C_4Li_{(n-1)\times8}}$ are the total energies of the monolayer with n and $(n-1)$ Li layers, respectively. The number '8' here corresponds to the totally eight adsorbed Li atoms in each Li layer (for one supercell on both sides). The calculated average adsorption energies for the first and the second layer are -0.50 and -0.02 eV, respectively. When still more Li layers are adsorbed, the layer-resolved adsorption energy will turn to be positive. It implies that then the Li metal cluster will begin to form, which prevents the further adsorption of the third Li layer. Hence the adsorption of Li atoms reach saturation after the formation of the second layer. Therefore, the 2×2 supercell could accommodate up to 16 Li atoms, and the corresponding chemical stoichiometry is Nb_2CLi_4. The evaluated average open circuit voltage decreases from 0.65 to 0.25 V with the increase of the adsorbed Li atoms. Compared with that of $Ti_3C_2Li_2$ (0.62 V[35]), the average open circuit voltage values of Nb_2CLi_4 are much

lower. The corresponding theoretical specific capacity of Nb_2C as electrodes for LIBs is 542 mA h g^{-1}, which is much larger than that of graphite (372 mA h g^{-1} for LiC_6). We note that although the Li storage capacity of Nb_2C is lower than that of V_2C,[41] they in fact both accommodate 16 Li atoms in one 2×2 supercell. The difference is due to the fact that the element Nb is heavier than V. This is in agreement with the corresponding experimental findings.[40] We also mention that the experimentally measured charge/discharge curves correspond to a dynamical process hence cannot be accurately determined by the equilibrium DFT approach employed here. Nevertheless, the obtained average open circuit voltages (corresponding to the endpoints of that curve) do provide a good estimate for the different materials.

For the rest of A′ atoms, namely Na, K, Mg and Ca atoms, we perform the calculations following the procedures described above. For Na and K, their chemical valences are both +1. We find that one supercell could accommodate up to 8 Na atoms and 4 K atoms, respectively. The corresponding chemical stoichiometries are Nb_2CNa_2 and Nb_2CK_1. The calculated average open circuit voltages and their corresponding theoretical specific capacities are 0.27 V and 271 mA h g^{-1} for Nb_2CNa_2, and 0.29 V and 136 mA h g^{-1} for Nb_2CK_1. As for Mg and Ca, their chemical valences are both +2. We find the bare Nb_2C supercell could accommodate up to 16 (two layers) Mg atoms but only 4 Ca atoms, respectively, with corresponding chemical stoichiometries Nb_2CMg_4 and Nb_2CCa_1. The calculated average open circuit voltages and their corresponding theoretical specific capacities are 0.18 V and 1084 mA h g^{-1} for Nb_2CMg_4, and 0.06 V and 271 mA h g^{-1} for Nb_2CCa_1. We note that although Nb_2C shows a fairly good capacity for Ca, when further considering the solid electrolyte interface (SEI) formation, due to the very low average open circuit voltage (0.06 V) for Nb_2CCa_1, the bare Nb_2C might not be a suitable anode material for Ca-ion batteries.

Typically the experimental samples would be a mixture of monolayer, few-layer, and even bulk materials. From experiment, it is observed that the interlayer distance is around 4 Å, which limits the amount of ions intercalated between the layers (and also decreases the diffusion efficiency). Therefore, to enhance the performance, appropriate methods need to be developed to decrease the thickness and to expose more surface area of the material.

From the above discussion, concerning the average open circuit voltage and the specific capacity, the bare Nb_2C monolayer is most suitable for anode materials of Li-ion and Mg-ion batteries.

4 Conclusions

In summary, we have studied the electronic properties and Li or non-Li storage capabilities of monolayer Nb_2C and its fluoride and hydroxide materials. We find that the Nb_2C monolayer and its derived Nb_2CF_2 and $Nb_2C(OH)_2$ in their the most stable configurations are all metallic before and after metal atom adsorption, which is the desired property of battery electrode materials. Among all the searched secondary batteries, the bare Nb_2C monolayer is most suitable as anode materials for Li-ion and Mg-ion batteries. It shows fast ion diffusion with very low diffusion barrier heights (<0.1 eV) and high storage capacities (with theoretical value 542 mA h g^{-1} for Li and 1084 mA h g^{-1} for Mg). In addition, we find that the functional groups tend to reduce the Li or non-Li capacity almost completely, which needs be avoided in experiment as much as possible. Moreover, the average intercalation potentials for Nb_2C-based materials are also found to be relatively low. Our results suggest that 2D Nb_2C is a promising anode material for Li- and non-Li-ion batteries.

Acknowledgements

References

1 B. Dunn, H. Kamath and J.-M. Tarascon, *Science*, 2011, **334**, 928–935.

2 H. Chen, T. N. Cong, W. Yang, C. Tan, Y. Li and Y. Ding, *Nat. Sci.*, 2009, **19**, 291–312.

3 D. Er, J. Li, M. Naguib, Y. Gogotsi and V. B. Shenoy, *ACS Appl. Mater. Interfaces*, 2014, **6**, 11173–11179.

4 J. B. Goodenough and Y. Kim, *Chem. Mater.*, 2010, **22**, 587–603.

5 M. D. Slater, D. Kim, E. Lee and C. S. Johnson, *Adv. Funct. Mater.*, 2013, **23**, 947–958.

6 H. Pan, Y.-S. Hu and L. Q. Chen, *Energy Environ. Sci.*, 2013, **6**, 2338–2360.

7 A. Eftekhari, *J. Power Sources*, 2004, **126**, 221–228.

8 C. D. Wessells, S. V. Peddada, R. A. Huggins and Y. Cui, *Nano Lett.*, 2011, **11**, 5421–5425.

9 N. Singh, T. S. Arthur, C. Ling, M. Matsui and F. Mizuno, *Chem. Commun.*, 2013, **49**, 149–151.

10 T. Ichitsubo, T. Adachi, S. Yagi and T. Doi, *J. Mater. Chem.*, 2011, **21**, 11764–11772.

11 D. Datta, J. Li and V. B. Shenoy, *ACS Appl. Mater. Interfaces*, 2014, **6**, 1788–1795.

12 S. Liu, J. J. Hu, N. F. Yan, G. L. Pan, G. R. Li and X. P. Gao, *Energy Environ. Sci.*, 2012, **5**, 9743–9746.

13 S. Jeong, D. Yoo, J. T. Jang, M. Kim and J. Cheon, *J. Am. Chem. Soc.*, 2012, **134**, 18233–18236.

14 K. G. Zhou, N. N. Mao, H. X. Wang, Y. Peng and H. L. Zhang, *Angew. Chem., Int. Ed.*, 2011, **50**, 10839–10842.

15 Z. Y. Zeng, Z. Y. Yin, X. Huang, H. Li, Q. Y. He, G. Lu, F. Boey and H. Zhang, *Angew. Chem., Int. Ed.*, 2011, **50**, 11093–11097.

16 M. Chhowalla, H. S. Shin, G. Eda, L.-J. Li, K. P. Loh and H. Zhang, *Nat. Chem.*, 2013, **5**, 263–275.

17 X. Zhao, C. M. Hayner, M. C. Kung and H. H. Kung, *ACS Nano*, 2011, **5**, 8739–8749.

18 J. Xiao, D. Choi, L. Cosimbescu, P. Koech, J. Liu and J. P. Lemmon, *Chem. Mater.*, 2010, **22**, 4522–4524.

19 Y. Jing, Z. Zhou, C. R. Cabrera and Z. Chen, *J. Mater. Chem. A*, 2014, **2**, 12104–12122.

20 Q. Tang and Z. Zhou, *Prog. Mater. Sci.*, 2013, **58**, 1244–1315.

21 Y. Li, D. Wu, Z. Zhou, C. R. Cabrera and Z. Chen, *J. Phys. Chem. Lett.*, 2012, **3**, 2221–2227.

22 Y. Jing, Z. Zhou, C. R. Cabrera and Z. Chen, *J. Phys. Chem. C*, 2013, **117**, 25409–25413.

23 L. David, R. Bhandavat and G. Singh, *ACS Nano*, 2014, **8**, 1759–1770.

24 M. Naguib, M. Kurtoglu, V. Presser, J. Lu, J. J. Niu, M. Heon, L. Hultman, Y. Gogotsi and M. W. Barsoum, *Adv. Mater.*, 2011, **23**, 4248–4253.

25 M. Naguib, V. N. Mochalin, M. W. Barsoum and Y. Gogotsi, *Adv. Mater.*, 2014, **26**, 992–1005.

26 O. Mashtalir, M. Naguib, V. N. Mochalin, Y. Dall'Agnese, M. Heon, M. W. Barsoum and Y. Gogotsi, *Nat. Commun.*, 2013, **4**, 1716–7.

27 M. Naguib, V. Presser, D. Tallman, J. Lu, L. Hultman, Y. Gogotsi and M. W. Barsoum, *J. Am. Ceram. Soc.*, 2011, **94**, 4556–4561.

28 M. Naguib, O. Mashtalir, J. Carle, V. Presser, J. Lu, L. Hultman, Y. Gogotsi and M. W. Barsoum, *ACS Nano*, 2012, **6**, 1322–1331.

29 O. Mashtalir, M. Naguib, B. Dyatkin, Y. Gogotsi and M. W. Barsoum, *Mater. Chem. Phys.*, 2013, **139**, 147–152.

30 M. Kurtoglu, M. Naguib, Y. Gogotsi and M. W. Barsoum, *MRS Commun.*, 2012, **2**, 133–137.

31 I. R. Shein and A. L. Ivanovskii, *Comput. Mater. Sci.*, 2012, **65**, 104–114.

32 A. N. Enyashin and A. L. Ivanovskii, *J. Solid State Chem.*, 2013, **207**, 42–48.

33 A. N. Enyashin and A. L. Ivanovskii, *J. Phys. Chem. C*, 2013, **117**, 13637–13643.

34 A. N. Enyashin and A. L. Ivanovskii, *Comput. Theor. Chem.*, 2012, **989**, 27–32.

35 Q. Tang, Z. Zhou and P. Shen, *J. Am. Chem. Soc.*, 2012, **134**, 16909–16916.

36 J. Come, M. Naguib, P. Rozier, M. W. Barsoum, Y. Gogotsi, P. L. Taberna, M. Morcrette and P. Simon, *J. Electrochem. Soc.*, 2012, **159**, A1368–A1373.

37 M. Naguib, J. Come, B. Dyatkin, V. Presser, P.-L. Taberna, P. Simon, M. W. Barsoum and Y. Gogotsi, *Electrochem. Commun.*, 2012, **16**, 61–64.

38 M. R. Lukatskaya, O. Mashtalir, C. E. Ren, Y. Dall'Agnese, P. Rozier, P. L. Taberna, M. Naguib, P. Simon, M. W. Barsoum and Y. Gogotsi, *Science*, 2013, **341**, 1502–1505.

39 Y. Xie, Y. Dall'Agnese, M. Naguib, Y. Gogotsi, M. W. Barsoum, H. L. Zhuang and P. R. Kent, *ACS Nano*, 2014, **8**, 9606–9615.

40 M. Naguib, J. Halim, J. Lu, K. M. Cook, L. Hultman, Y. Gogotsi and M. W. Barsoum, *J. Am. Chem. Soc.*, 2013, **135**, 15966–15969.

41 J. P. Hu, B. Xu, C. Y. Ouyang, S. Y. A. Yang and Y. G. Yao, *J. Phys. Chem. C*, 2014, **118**, 24274–24281.

42 J. Ihm, A. Zunger and M. L. Cohen, *J. Phys. C: Solid State Phys.*, 1979, **12**, 4409–4421.

43 J. P. Perdew, K. Burke and M. Ernzerhof, *Phys. Rev. Lett.*, 1996, **77**, 3865–3868.

44 G. Kresse and D. Joubert, *Phys. Rev. B: Condens. Matter*, 1999, **59**, 1758–1775.

45 G. Kresse and J. FurthmÍźller, *Phys. Rev. B: Condens. Matter*, 1996, **54**, 11169–11186.

46 V. I. Anisimov, I. V. Solovyev and M. A. Korotin, *Phys. Rev. B: Condens. Matter*, 1993, **48**, 16929–16934.

47 V. I. Anisimov, F. Aryasetiawan and A. I. Lichtenstein, *J. Phys.: Condens. Matter*, 1997, **9**, 767–808.

48 H. Xu, A. Chernatynskiy, D. Lee, S. B. Sinnott, V. Gopalan, V. Dierolf and S. R. Phillpot, *Phys. Rev. B: Condens. Matter Mater. Phys.*, 2010, **82**, 184109.

49 H. J. Monkhorst and J. D. Pack, *Phys. Rev. B: Solid State*, 1976, **13**, 5188–5192.

50 M. Khazaei, M. Arai, T. Sasaki, C. Y. Chung, N. S. Venkataramanan, M. Estili, Y. Sakka and Y. Kawazoe, *Adv. Funct. Mater.*, 2013, **23**, 2185–2192.

51 G. Henkelman, B. P. Uberuaga and H. Jónsson, *J. Chem. Phys.*, 2000, **113**, 9901–9904.

52 J. Setiadi, D. A. Matthew and J. F. Michael, *ACS Appl. Mater. Interfaces*, 2013, **5**, 10690–10695.

53 X. X. Guo, P. Guo, J. M. Zheng, L. K. Cao and P. J. Zhao, *Appl. Surf. Sci.*, 2015, **341**, 69–74.

54 X. Lin and J. Ni, *Phys. Rev. B: Condens. Matter Mater. Phys.*, 2012, **86**, 075440.

55 X. Fan, W. T. Zheng and J. L. Kuo, *ACS Appl. Mater. Interfaces*, 2012, **4**, 2432–2438.

56 L. J. Zhou, Z. F. Hou and L. M. Wu, *J. Phys. Chem. C*, 2012, **116**, 21780–21787.

57 C. Ling and F. Mizuno, *Phys. Chem. Chem. Phys.*, 2014, **16**, 10419–10424.

58 K. T. Chan, J. B. Neaton and M. L. Cohen, *Phys. Rev. B: Condens. Matter Mater. Phys.*, 2008, **77**, 235430.

59 G. C. Guo, X. L. Wei, D. Wang, Y. Luo and L. M. Liu, *J. Mater. Chem. A*, 2015, **3**, 11246–11252.

60 S. Zhao, W. Kang and J. Xue, *J. Mater. Chem. A*, 2014, **2**, 19046–19052.

61 V. V. Kulish, O. I. Malyi, C. Persson and P. Wu, *Phys. Chem. Chem. Phys.*, 2015, **17**, 13921–13928.

62 T. Hu and J. S. Hong, *J. Phys. Chem. C*, 2015, **119**, 8199–8207.

63 M. Mortazavi, C. Wang, J. Deng, V. B. Shenoy and N. V. Medhekar, *J. Power Sources*, 2014, **268**, 279–286.

64 S. Q. Yang, D. X. Li, T. R. Zhang, Z. L. Tao and J. Chen, *J. Phys. Chem. C*, 2012, **116**, 1307–1312.

65 M. V. Koudriachova, N. M. Harrison and S. W. de Leeuw, *Phys. Rev. Lett.*, 2001, **86**, 1275.

66 M. Wagemaker, R. van de Krol, A. P. Kentgens, A. A. Van Well and F. M. Mulder, *J. Am. Chem. Soc.*, 2001, **123**, 11454–11461.

67 Y. S. Wang, X. Q. Yu, S. Y. Xu, J. M. Bai, R. J. Xiao, Y. S. Hu, H. Li, X. Q. Yang, L. Q. Chen and X. J. Huang, *Nat. Commun.*, 2013, **4**, 2365.

68 K. Persson, Y. Hinuma, Y. S. Meng, A. Van der Ven and G. Ceder, *Phys. Rev. B: Condens. Matter Mater. Phys.*, 2010, **82**, 125416.

69 M. K. Aydinol and G. Ceder, *J. Electrochem. Soc.*, 1997, **144**, 3832–3835.

70 Y. S. Meng, *Energy Environ. Sci.*, 2009, **2**, 589–609.